catalysts

MDPI

*Article*

# Preparation of a Novel NiAlO Composite Oxide Catalyst for the Dehydrogenation of Methylcyclohexane

**Dongliang Wang †, Qian Lei †, Hongwei Li, Guixian Li and Yu Zhao ***

School of Petrochemical Engineering, Lanzhou University of Technology, Lanzhou 730050, China
* Correspondence: yzhao@lut.edu.cn; Tel.: +86-931-7823125; Fax: +86-931-7823001
† These authors contributed equally to this work.

**Abstract:** A series of NiAlO composite oxide catalysts with high surface areas and high Ni dispersion were prepared through an improved co-precipitation method. The new preparation method effectively improved the specific surface area and pore volume of the catalyst, promoted the dispersion of nickel species, alleviated the agglomeration of the catalyst, and improved the stability of the catalyst by strengthening the interaction between Ni and Al. The typical catalyst $Ni_{20}Al$ had a specific surface area of 359 $m^2/g$ and a $NiAl_2O_4$ phase. In the dehydrogenation of methylcyclohexane over the $Ni_{20}Al$ catalyst, the conversion of methylcyclohexane could reach 77.4%, with toluene selectivity of 85.6%, and a hydrogen release rate of 63.94 mmol $g^{-1}$ $h^{-1}$, and did not show any significant inactivation during the stability test over 29 h under the reaction conditions of reaction temperature 450 °C and LHSV = 4 mL $g^{-1}$ $h^{-1}$. However, the conversion of methylcyclohexane with the IM-NiAl catalyst prepared through the traditional impregnation method was only 50.75%, with toluene selectivity of 70.5%, and with a hydrogen release rate of 35.84 mmol $g^{-1}$ $h^{-1}$, and the lifetime of the catalyst was only 15 h.

**Keywords:** nickel-based catalyst; dehydrogenation; methylcyclohexane; toluene; specific surface area



**Citation:** Wang, D.; Lei, Q.; Li, H.; Li, G.; Zhao, Y. Preparation of a Novel NiAlO Composite Oxide Catalyst for the Dehydrogenation of Methylcyclohexane. *Catalysts* **2022**, *12*, 958. https://doi.org/10.3390/catal12090958

Academic Editors: Leonarda Francesca Liotta and Fan Zhang

Received: 29 July 2022
Accepted: 26 August 2022
Published: 29 August 2022



## 1. Introduction

With the rapid development of the social economy, human society is facing serious problems such as the energy shortage and environmental pollution. As a renewable energy with abundant reserves, hydrogen energy has the advantages of high calorific value and being pollution-free. It is one of the most ideal clean energies at present [1]. Due to the limitations of hydrogen storage and transportation technology, hydrogen energy has still not been applied in the large-scale industry [2]. Effective development of a safe and efficient hydrogen storage and transportation technology is very important for the large-scale application of hydrogen energy [3]. Currently, commonly used hydrogen storage technologies mainly include high-pressure gaseous hydrogen storage, low-temperature liquid hydrogen storage, adsorption hydrogen storage, metal material hydrogen storage, and organic liquid hydride hydrogen storage [4,5]. Compared with other hydrogen storage technologies, organic liquid hydride storage has many advantages, such as high hydrogen storage density of organic liquid hydride and liquid state at room temperature, and atmospheric pressure, which greatly facilitate its storage and transportation. At present, the most suitable organic hydride hydrogen storage materials are aromatics and aromatic derivatives, which have higher hydrogen storage density and better reaction reversibility than unsaturated olefins, alkynes, cyclohexane, methylcyclohexane, naphthane, ethyl carbazole, and other aromatics [6]. Among them, methylcyclohexane (MCH) is one of the organic representative hydrides, and its hydrogen storage mass and bulk density reach 6.5 wt% and 47.4 g $L^{-1}$, respectively [7]. Organic liquid hydride storage technology is the most likely technology to realize industrial production and application in the existing technology. However, because the dehydrogenation reaction is a strong endothermic reaction,

which needs to absorb a lot of heat in the reaction process, it is very easy to destroy the structure of the catalyst under high-temperature conditions and make the catalyst cook and deactivate [8,9]; therefore, it is of great significance to develop a low-temperature and efficient organic liquid hydride dehydrogenation catalyst. Nowadays, the active components of dehydrogenation catalysts are mainly Pt, Pd, Ir, Ni, etc. [10–13]. Among these, Pt has an excellent catalytic performance, which has attracted extensive attention from researchers. Wu et al. [14] designed a series of Pt/Mg-Al-O catalysts. Under the reaction temperature of 623 K, the MCH dehydrogenation conversion was measured to reach 98.0%. Yukihiro et al. [15] prepared a series of $Pt/TiO_2$-$Al_2O_3$ catalysts, over which the MCH dehydrogenation conversion reached 95.0% under the reaction temperature of 608 K and LHSV = 1.5 $h^{-1}$. Li et al. [16] synthesized activated carbon-supported Pt catalysts, over which the MCH dehydrogenation conversion was measured to reach 88% and the lifetime of the catalyst was about 24 h under the reaction temperature of 573 K and the MCH flow rate of 1.8 mL/h. However, its disadvantages, such as high cost, instability at high temperatures, easy cooking, etc., greatly limit its application in the industry. Ni-based catalysts have a low price and good catalytic performance, and have also attracted much attention in recent years. Chen et al. [17] used 20% $Ni/\gamma$-$Al_2O_3$ as a catalyst; under the reaction temperature of 673 K, the flow rate of MCH of 1 mL/h, and the hydrogen partial pressure of 0.5 MPa, the MCH dehydrogenation conversion was measured to be 94.55%. Gulyaeva et al. [18] designed high-loaded nickel-based sol–gel catalysts; under the reaction temperature of 548 K, the flow rate of MCH of 12 mL/h, and the hydrogen partial pressure of 0.1 MPa, the MCH dehydrogenation conversion was 75% and the lifetime of the catalyst was only 20 h. Hyungwon et al. [19] designed a series of Si(x)-$Ni/SiO_2$ catalysts, over which the MCH dehydrogenation conversion was 45.0% at 623 K and GHSV = 25,000 $h^{-1}$. Yolcular [20] designed a series of $NiSiO_2$ catalysts, over which the MCH dehydrogenation conversion was 90.0% at 713 K. Anaam [21] used $NiZn/Al_2O_3$ as a catalyst with the reaction temperature of 673 K, where the MCH dehydrogenation conversion was only 10%, but the toluene selectivity was 99.5%. However, there were still problems such as short service life and easy agglomeration for the Ni-based catalysts [22]. Therefore, it is of great significance to improve the activity and stability of the catalyst by preparing a catalytic system with a high surface area and high dispersion. In this paper, the precursor of the Ni-O-Al catalyst was prepared through a simple improved co-precipitation method. The precursor of the catalyst was treated with n-butanol, which improved the specific surface area of the catalyst and increased the dispersion of the active component. In addition, there was a strong interaction between Ni and Al, which inhibits the agglomeration of the active component Ni.

## 2. Results and Discussion

### *2.1. $N_2$ Adsorption-Desorption Measurement*

The $N_2$ adsorption-desorption isotherms and pore size distribution curves of the catalysts are shown in Figure 1a,b, and the specific surface areas, pore volumes, and pore size distribution data of the calcined samples are listed in Table 1. From Figure 1a, it can be seen that the adsorption amount of the IM-NiAl catalyst was small, while the $Ni_xAl$ series catalysts had a larger adsorption amount compared with the IM-NiAl catalyst, and all showed IV-type isotherms and H3-type hysteresis loops [23]. From Figure 1b, it can be seen that $Ni_{10}Al$ and $Ni_{15}Al$ samples exhibited the large and widely distributed pores around 15 nm, while the $Ni_{20}Al$ sample possessed widely distributed bimodal pores around 6 and 17 nm; however, for the $Ni_{25}Al$ and IM-NiAl samples, the pore size distributions were relatively diffuse. The specific surface area of $Ni_xAl$ catalysts increased and then decreased with the increase in Ni content, and the maximum specific surface area was 480 $m^2/g$ at 15 wt% Ni content. The increase of Ni content will promote the formation of composite oxide with skeleton structure and thus increase the specific surface area, but the excessive Ni content will lead to the agglomeration of Ni particles and block the pore channels, resulting in the decrease in the specific surface area.

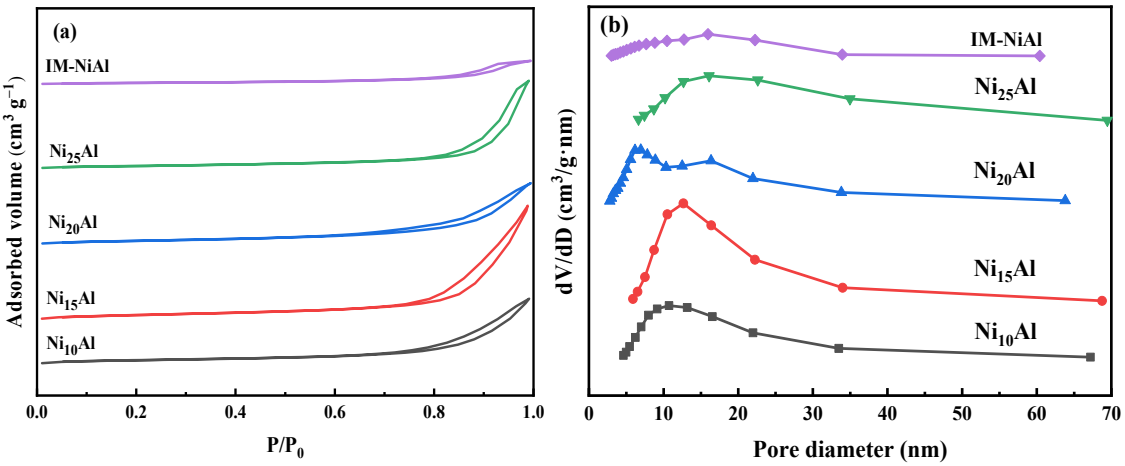


**Figure 1.** (**a**) $N_2$ adsorption and desorption isotherms and (**b**) pore size distribution curves of catalyst samples.

**Table 1.** Physicochemical properties of $Ni_xAl$ and IM-NiAl catalysts.

| Catalyst | Ni Content/wt% | Specific Surface Area /($m^2$/g) | Pore Size/nm |
|---|---|---|---|
| $Ni_{10}Al$ | — | 400 | 13.44 |
| $Ni_{15}Al$ | — | 480 | 18.17 |
| $Ni_{20}Al$ | 18.78 | 359 | 13.99 |
| $Ni_{25}Al$ | — | 272 | 10.12 |
| IM-NiAl | 19.63 | 133 | 16.29 |

The $Ni_xAl$ catalysts prepared by the modified co-precipitation method have large specific surface areas, which are mainly due to the synthesis of Ni-O-Al skeletal structure precursors by controlling the pH value of the precipitation and treating the precursors by the evaporation of n-butanol, which enlarges the pore size and pore volume of the catalyst, thus increasing the specific surface area and the dispersion of the metal. This has been reported in our previous studies [24,25]. Although the $Ni_{15}Al$ catalyst prepared by the co-precipitation method had the largest specific surface area, the nickel content in the catalyst also had a greater effect on the reaction for the methylcyclohexane dehydrogenation reaction, and the $Ni_{20}Al$ catalyst was found to be the most effective for dehydrogenation through preliminary exploration (see later). Therefore, the nickel content of the comparison sample prepared by impregnation was chosen to be consistent with the $Ni_{20}Al$ catalyst. The specific surface area and pore volume of the IM-NiAl catalyst prepared with the commercial alumina as support were found to be greatly reduced compared with the support, with a specific surface area of 133 $m^2/g$ and a pore volume of 0.54 $cm^3/g$. This also indicates that the metal particles of the catalyst prepared by the impregnation method were agglomerated, leading to pore blockage, and greatly affecting the activity of the catalyst. In contrast, the specific surface area and pore volume of the $Ni_xAl$ catalyst prepared by the improved co-precipitation method was significantly improved. The high specific surface area and large pore volume can increase the number of attachment sites for the active components, be beneficial for the high dispersion of metal species, and improve the utilization rate of the active components of the catalyst.

### *2.2. Determination of Nickel Content in Catalyst*

ICP was used to determine the actual nickel content of the calcined catalyst, and the results are listed in Table 1. The theoretical nickel contents of the catalysts $Ni_{10}Al$, $Ni_{15}Al$, $Ni_{20}Al$, and $Ni_{25}Al$ were 10 wt%, 15 wt%, 20 wt%, and 25 wt%, respectively. The actual nickel content of the typical catalyst $Ni_{20}Al$ (18.78 wt%) was close to the theoretical value, which shows that the preparation method was suitable, and nickel ions can mostly

precipitate in the preparation process. In addition, the IM-NiAl catalyst possessed almost the same nickel content (19.63 wt%) as that of $Ni_{20}Al$, as expected.

### *2.3. XRD*

Figure 2a shows the XRD patterns of the roasted $Ni_xAl$ and IM-NiAl catalysts. Only the characteristic diffraction peaks of the $NiAl_2O_4$ spinel phase were observed in the XRD patterns of the roasted $Ni_xAl$ catalysts, and no characteristic diffraction peaks associated with the NiO species were observed, indicating that the skeletal structure of NiAlO composites was synthesized by the modified co-precipitation method, and that strong interactions between nickel and aluminum existed. The nickel species were highly dispersed in the composite skeleton and no significant agglomeration was observed even with the increase in metal content. Furthermore, the XRD patterns of IM-NiAl catalysts showed sharp NiO characteristic diffraction peaks at 2θ = 37.3°, 47.3°, 62.8°, and 75.3° (PDF#75-0269), indicating the presence of large particles of nickel oxide species in the IM-NiAl catalyst prepared by the impregnation method compared with that of the $Ni_{20}Al$ catalyst with almost the same Ni content.

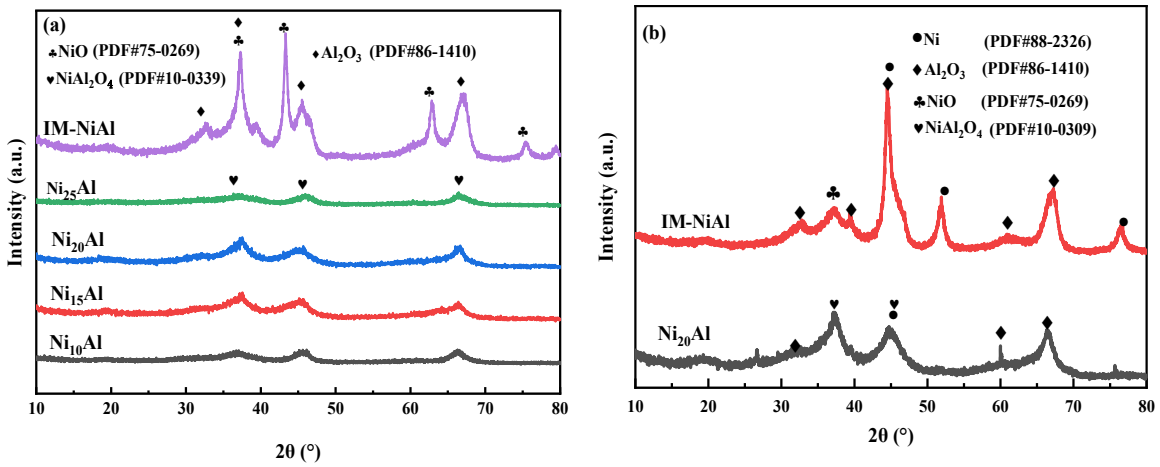


**Figure 2.** XRD patterns of $Ni_xAl$ and IM-NiAl catalysts: (**a**) after calcination and (**b**) after reduction.

Figure 2b shows the XRD patterns of the reduced $Ni_{20}Al$ and IM-NiAl catalysts with almost the same Ni content. The $Ni_{20}Al$ catalyst prepared by the modified co-precipitation method showed a weak characteristic diffraction peak at 2θ = 44.6° ascribed to $Ni^0$ (PDF#88-2326) and diffraction peak at 2θ = 37.3° and 44.6° ascribed to $NiAl_2O_4$ (PDF#10-0309), while the IM-NiAl catalyst prepared by the impregnation method showed sharp characteristic diffraction peaks of Ni at 2θ = 44.6°, 51.9°, and 76.8° (PDF# 88-2326), and weak characteristic diffraction peaks of NiO at 2θ = 37.3°. This indicated that the IM-NiAl catalyst prepared by the impregnation method possessed some agglomeration of Ni species after a high-temperature reduction. Compared with the conventional impregnation method, the catalyst prepared by the improved co-precipitation method had a large specific surface area, which provided a better dispersion base for the active components. The treatment of the precursor by n-butanol could effectively prevent the adhesion of the particles and expand the pores and increase the capacity. In addition, the regular arrangement of Ni in the spinel structure formed in the $Ni_xAl$ catalysts could suppress Ni sintering, which led to the smaller Ni particles. These results agreed well with the TEM result below and further largely alleviated the agglomeration of the nickel species during the reaction and greatly extended the catalyst lifetime [26].

### *2.4. TEM Analysis*

Figure 3a,b show the TEM images and particle size statistics of the reduced $Ni_{20}Al$ catalyst and IM-NiAl catalyst, respectively. The average particle size of the $Ni_{20}Al$ catalyst

was found to be only 2.13 nm, while the obvious agglomeration of nickel species in the IM-NiAl catalyst prepared by the impregnation method was clearly observed in Figure 3b. The average particle size of the IM-NiAl catalyst was found to be 11.24 nm and the dispersion of nickel species on the catalyst surface was extremely poor. Thus, TEM results clearly reveal that the catalysts prepared by the modified co-precipitation method had smaller particle sizes and better dispersion of metal species than those prepared by the impregnation method.

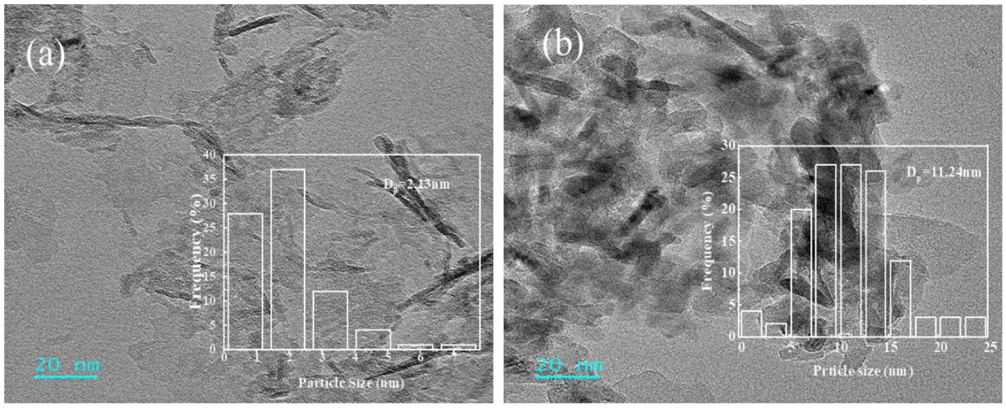


**Figure 3.** TEM images and particle size distribution of $Ni_{20}Al$ (**a**) and IM-NiAl catalysts (**b**).

### *2.5. XPS Analysis*

Figure 4 shows the XPS spectra of the reduced $Ni_{20}Al$ and IM-NiAl catalysts. The peak around 857.9 eV for Ni $2p_{3/2}$ was attributed to the $Ni^{2+}$ species in the surface of the catalyst, indicating the presence of $Ni^{2+}$ in the reduced $Ni_{20}Al$ and IM-NiAl [27]. The peak at 863.5 eV was the satellite of Ni $2p_{3/2}$. In general, the binding energy peak position of $Ni^{2+}$ $2p_{3/2}$ of NiO was located around 855.8 eV, and the satellite peak binding energy peak position at the edge of $Ni^{2+}$ $2p_{3/2}$ was located at 861.8 eV. The shift of the binding energy to a higher position for the reduced $Ni_{20}Al$ and IM-NiAl catalyst indicated that there was an interaction between the nickel species and the carrier alumina [28,29], which was also verified by the XRD results above. In addition, a peak of $Ni^0$ was observed in the XPS spectra of both the reduced $Ni_{20}Al$ catalyst and the IM-NiAl catalyst, indicating that a fraction of NiO was reduced. The peak splitting process was performed on the Auger spectrum, and the results showed that the $Ni^{2+}$ content in the $Ni_{20}Al$ catalyst was 60.43%, while the $Ni^{2+}$ content in the IM-NiAl catalyst prepared by the impregnation method was 45.81%. The results indicate that the nickel species in the IM-NiAl catalyst had a relatively weak interaction with the carrier and was easily reduced to $Ni^0$, which made the IM-NiAl catalyst prone to agglomeration during the reaction. Furthermore, the $Ni_{20}Al$ catalyst contained more $NiAl_2O_4$ crystalline phases with a stronger interaction between the nickel species and the carrier, which limited the reduction of $Ni^{2+}$.

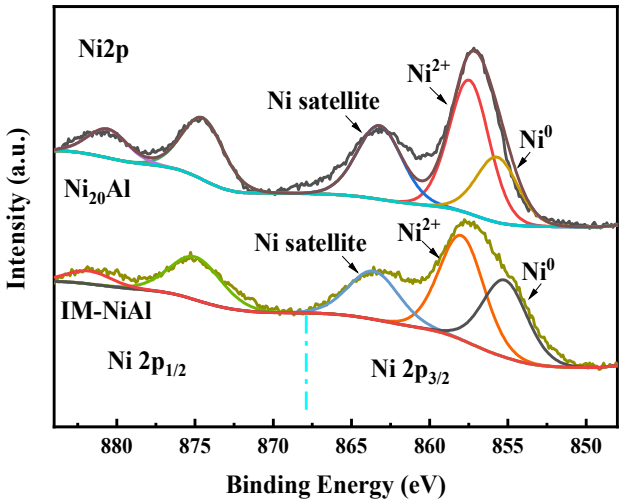


**Figure 4.** Ni XPS spectra of the reduced $Ni_{20}Al$ and IM-NiAl.

### *2.6. Catalytic Performance in the Dehydrogenation of MCH*

The catalytic performances for the $Ni_xAl$ series catalysts were tested with the dehydrogenation of methylcyclohexane to toluene as the probe reaction, which was carried out in a fixed bed reactor. Based on our previous results, the LHSV of 4 mL $g^{-1}$ $h^{-1}$ was more suitable for this reaction, thus the LHSV was just chosen at 4 mL $g^{-1}$ $h^{-1}$ in this paper.

The effects of the nickel content of the $Ni_xAl$ series catalysts and temperature on the dehydrogenation of MCH were firstly studied and the results are shown in Figure 5. At the same temperature, the conversion of MCH increased and then decreased with the increase in the nickel content of the $Ni_xAl$ series catalysts. Specifically, the conversion of MCH was gradually increased when the nickel content increased from 10% to 20%, but began to decrease when the nickel content continued to increase. The main reason was that with the nickel content increased, the nickel was uniformly dispersed on the carrier, providing enough active sites for the catalyst, and thus increasing the catalyst activity; however, as the nickel content continued to increase, it led to a rapid decrease in the specific surface area of the carrier, which could not provide enough active sites for the active center, resulting in a large amount of nickel agglomeration, and thus reducing the activity of the catalyst. Therefore, the optimum nickel content of the catalyst was 20%. Subsequently, at the same nickel content, the effect of the reaction temperature on the dehydrogenation of MCH over the $Ni_{20}Al$ catalysts prepared by the modified co-precipitation method and the IM-NiAl catalysts prepared by the conventional impregnation method was studied. The results showed that the conversion of MCH firstly increased and then decreased with the increase in the reaction temperature. This phenomenon is due to the fact that the MCH dehydrogenation is a heat-absorbing reaction, thus the conversion of MCH increased with the elevation of temperature at the beginning step. The conversion of MCH over the IM-NiAl catalyst prepared by the impregnation method was only 50.7% at an LHSV of 4 mL $g^{-1}$ $h^{-1}$ and a reaction temperature of 450 °C, while that was up to 77.4% for the $Ni_{20}Al$ catalyst prepared by a modified co-precipitation method under the same conditions, which was mainly due to the larger specific surface area, smaller particle size, and better dispersion of the $Ni_{20}Al$ catalyst.

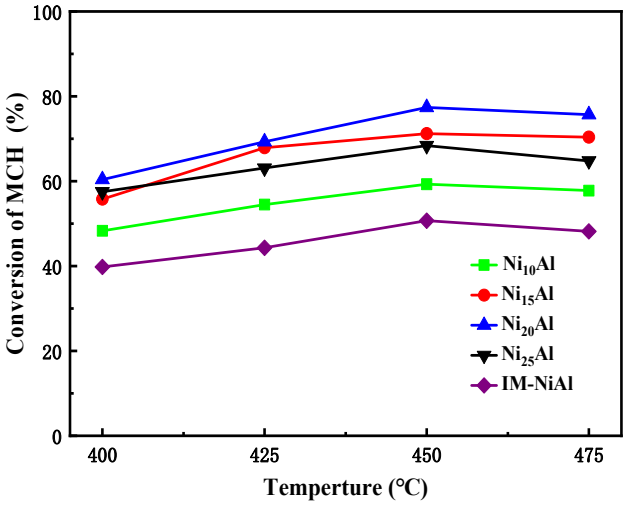


**Figure 5.** Effect of Ni content on dehydrogenation conversion of MCH.

The toluene selectivity over the typical $Ni_{20}Al$ catalyst and IM-NiAl catalyst at different temperatures is shown in Figure 6. It can be seen that the toluene selectivity of both catalysts exhibited the same trend as the conversion rate, with increasing and then decreasing as the temperature increased. At the optimized temperature of 450 °C, the toluene selectivity for the $Ni_{20}Al$ catalyst prepared by the improved co-precipitation method (85.6%) was significantly higher than that for the IM-NiAl catalyst prepared by the conventional impregnation method (70.5%).

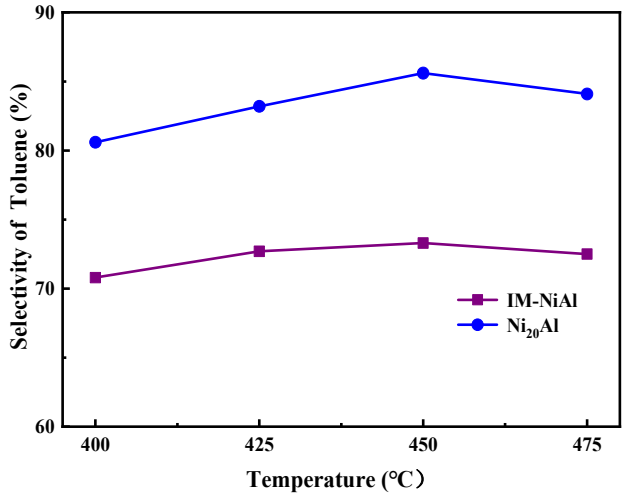


**Figure 6.** Toluene selectivity over the $Ni_{20}Al$ and IM-NiAl catalysts at different temperatures.

The hydrogen release rates in the dehydrogenation of MCH at different temperatures over the $Ni_{20}Al$ and IM-NiAl catalysts are shown in Figure 7. It increased and then decreased with the gradual increase in temperature over both the catalysts. The hydrogen release rate over the $Ni_{20}Al$ catalyst increased from 47.01 to 63.94 mmol $g^{-1}$ $h^{-1}$ at the range of 400–450 °C, but started to decrease after the temperature was further increased. The optimized hydrogen release rate over the $Ni_{20}Al$ catalyst was 61.47 mmol $g^{-1}$ $h^{-1}$, which is superior to that of the IM-NiAl catalyst prepared by the conventional impregnation method (35.84 mmol $g^{-1}$ $h^{-1}$).

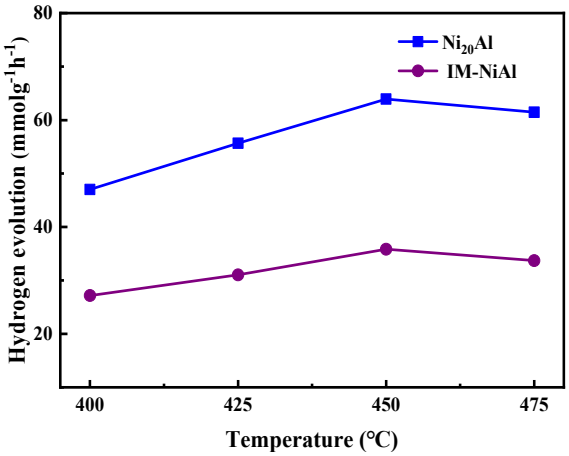


**Figure 7.** Hydrogen release rates over the $Ni_{20}Al$ and IM-NiAl catalysts at different temperatures.

Figure 8 shows the stability test results of the IM-NiAl and $Ni_{20}Al$ catalysts. The stability of the IM-NiAl and $Ni_{20}Al$ catalysts was tested under the conditions of T = 450 °C and LHSV = 4 mL $g^{-1}$ $h^{-1}$. It can be seen from the figure that the activity of the IM-NiAl catalyst prepared by the impregnation method was significantly decreased only after 15 h of reaction, while the activity of the $Ni_{20}Al$ catalyst prepared by a modified co-precipitation method was able to operate stably for 29 h, and then began to decrease.

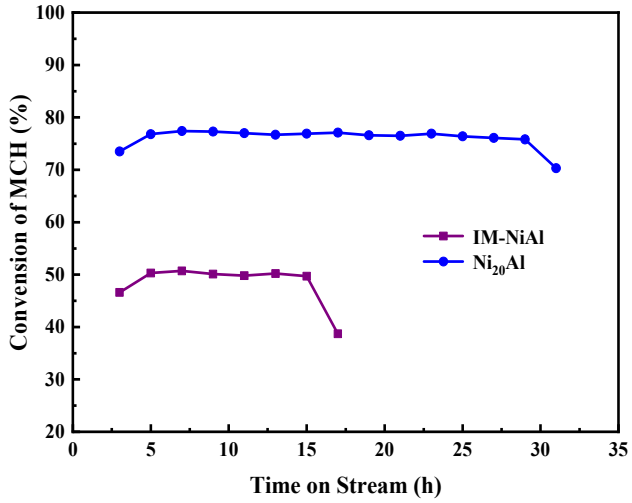


**Figure 8.** Stability test of IM-NiAl and $Ni_{20}Al$ catalysts.

Table 2 compares the performances of the catalysts for the dehydrogenation of MCH in this work with the results of previous literature. It can be seen that the $Ni_{20}Al$ catalyst showed higher catalytic activity than many reported Ni-based catalysts [19,30], and comparable catalytic activity with some Pt catalysts [31,32]. Although the Ni-Cu/$\gamma$-$Al_2O_3$-$ZrO_2$ catalyst [33] exhibited higher dehydrogenation activity than that of the $Ni_{20}Al$ catalyst used in this work, it contained complex compositions and more control points in the preparation process. Thus, the $Ni_{20}Al$ catalyst is a good candidate catalyst for dehydrogenation reaction due to its large specific surface area, high Ni dispersion, and simple preparation method.

**Table 2.** Comparison of the performance of the catalyst for dehydrogenation of methylcyclohexane in this work with the results of previous literature.

| Catalyst | T (K) | Conversion of MCH (%) | Selectivity of Toluene (%) | Reference |
|---|---|---|---|---|
| $Ni_{20}Al$ | 723 | 77.4 | 85.6 | This work |
| Si(x)-Ni/$SiO_2$ | 623 | 45 | 35 | [19] |
| Ni/$Al_2O_3$ | 653 | 55.23 | 99.9 | [30] |
| Ni-Cu/$\gamma$-$Al_2O_3$-$ZrO_2$ | 723 | 82.6 | 98.2 | [33] |
| Pt/$Al_2O_3$ | 623 | 71.2 | 97.1 | [31] |
| Pt-Sn/Mg-Al-O | 623 | 90.5 | 98.4 | [32] |

## 3. Experimental

### *3.1. Materials*

Methyl cyclohexane, toluene, methyl cyclohexene, nickel nitrate, aluminum nitrate, sodium carbonate, n-butanol, and absolute ethanol, all with an analytical grade, were purchased from Sinopharm Chemical Reagent Co., Ltd. (Shanghai, China).

### *3.2. Catalyst Preparation*

#### 3.2.1. Preparation of $Ni_xAl$ Catalyst

The $Ni_xAl$ catalyst was prepared through the improved co-precipitation method. Taking the sample with Ni content of 20% as an example, 37.5 g $Al(NO_3)_3 \cdot 9H_2O$, 6.3069 g $Ni(NO_3)_2 \cdot 6H_2O$ were dissolved in 100 mL distilled water, and 21.2 g $Na_2CO_3$ was dissolved in another 100 mL distilled water. Additionally, 400 mL deionized water was added to a 1L three-necked flask and heated to 90 °C under stirring, and then the two solutions above were added dropwise into this flask simultaneously under vigorous stirring at 90 °C (the final pH value of the solution was about 8). The solution was continuously stirred for 0.5 h, then the stirring was turned off, and let stand and aged at 90 °C for 12 h. Subsequently, the mixture was filtered, and the filter cake was washed with distilled water many times until to neutral, and then washed with anhydrous ethanol three times. 200 mL n-butanol was added into the solid obtained and evaporated at 110 °C. The solid was subsequently transferred to the oven for further drying at 110 °C for 12 h. Finally, the obtained sample was roasted at 500 °C in the muffle furnace (Nanjing Boyunton Instrument Technology Company, Nanjing, China) for 4 h to obtain NiAlO composite oxide, grounded into 40–60 mesh particles, and designated as $Ni_xAl$, in which x = 10%, 15%, 20%, and 25%, corresponded to the feeding content of Ni, respectively.

#### 3.2.2. Preparation of IM-NiAl Catalyst

For comparison, an IM-NiAl catalyst was prepared by the traditional impregnation method with the Ni content same as that of $Ni_{20}Al$ above. A commercial alumina (Suzhou yuante new material company, Suzhou, China) with a specific surface area of 450 $m^2/g$ and a pore volume of 1.8 $cm^3/g$ was the carrier. In total, 8 g of alumina powder was added to an appropriate amount of $Ni(NO_3)_2 \cdot 6H_2O$ aqueous solution, stirred for 0.5 h, placed in an ultrasonic environment for 2 h, then dried at 120 °C for 12 h. The powder was calcined at 500 °C in a muffle furnace for 4 h, and the solid obtained was recorded as the IM-NiAl catalyst.

### *3.3. Characterization*

X-ray diffraction (XRD) patterns were obtained on a D8 Advance diffractometer (Bruker (Beijing) Technology Company, Beijing, China) equipped with Cu K$\alpha$ radiation (40 kV, 40 mA), and scanning at a rate of 10°/min in the range from 10° to 80°. The diffraction pattern was analyzed to obtain information on the composition, molecular or atomic structure, and morphology inside the material.

Transmission electron microscopy (TEM) images were monitored via a Philips Tecnai G2 F20 microscope (FEI Company, OR, USA) operated at an accelerating voltage of

200 kV, which was utilized to analyze the morphology of the specimens. The catalyst was crushed and ground before testing, and the catalyst powder was dispersed in ethanol using ultrasound for 30 min. The particle size distribution of metal particles on the catalyst was counted using the analysis software Nano measurer, and 60 metal particles were selected on each TEM photograph.

Nitrogen adsorption-desorption isotherms were recorded on a Micromeritics ASAP 2460 automated physisorption instrument (Micromeritics Instrument Company, Norcross, GA, USA) at a liquid $N_2$ temperature of –196 °C. Before investigation, each sample was outgassed at 250 °C for 7 h. The total surface areas ($S_{BET}$) were derived from the Brunauer-Emmett-Teller (BET) method, whereas the total pore volume ($V_{total}$) was determined by the $N_2$ absorption amounts at $p/p_0 = 0.99$. The pore size distribution was obtained from the adsorption branch of the isotherms applying the Barrett-Joyner-Halenda (BJH) method.

The Aglient 5110 inductively coupled plasma (ICP) emission spectrometer from Agilent, Santa Clara, CA, USA was used to determine the nickel content of the catalysts prepared in this paper.

An X-ray photoelectron spectrometer (XPS) characterization was performed on a Thermo Scientific K-Alpha + X-ray photoelectron spectrometer (Thermo Fisher Scientific, Waltham, MA, USA) equipped with a monochromatic Al Ka X-ray source (hν = 1486.6 eV). The samples were pre-reduced in the laboratory and the reduced catalysts were encapsulated in centrifuge tubes. Before testing, the catalyst surface was etched with a high-energy electron beam to remove the oxide layer on the surface with an etch thickness of 3 nm.

### *3.4. Catalyst Evaluation*

The methylcyclohexane dehydrogenation reaction was conducted in a fixed-bed reactor at 400–475 °C, which was equipped with a thermocouple placed coaxially in the middle of the catalyst bed to monitor the temperature, under atmospheric pressure (shown in Figure 9). For each experiment, the 0.6 g catalyst, which was sieved to 40–60 mesh and mixed with 5 g inert arenaceous quartz of the same size, was loaded into the middle part of a stainless-steel reactor with an 8 mm internal diameter and total length of 500 mm. Before the start of the methylcyclohexane dehydrogenation reaction, the catalyst was first reduced at 450 °C for 4 h in high-purity $H_2$ at a flow rate of 70 mL/min, which was controlled by a mass flow controller. Methylcyclohexane (reagent) was fed into the reactor through a syringe pump with the rate of 2.4 mL/h. During the reaction process, the flow rate of $H_2$; as the carrier gas was maintained at 50 mL/min. The reaction products were analyzed on an online gas chromatograph (GC-2018) with a flame ionization detector (FID) using an SE-30 capillary column (50 m × 0.32 mm × 1 μm). The by-product was mainly methylcyclohexen and the selectivity of methylcyclohexene was 100% minus the amount of toluene; thus in this paper, we only needed to give the selectivity of toluene. The conversion of methylcyclohexane, the selectivity of the main product toluene, and the rate of hydrogen release from the catalyst were calculated as follows:

$$\text{Conversion of methylcyclohexane} = \frac{\text{MCH}_{\text{feed}} - \text{MCH}_{\text{off}}}{\text{MCH}_{\text{feed}}} \quad (1)$$

$$\text{Selectivity of toluene} = \frac{\text{Toluene}}{\text{MCH}_{\text{feed}} - \text{MCH}_{\text{off}}} \times 100\% \quad (2)$$

$$\text{Hydrogen release rate} = 3 \times 60 \times \frac{\text{u} \times \rho}{\text{m} \times \text{M}} \times \text{C} \times \text{S} \quad (3)$$

The meaning of each symbol in the formula is as follows:

u is the feed rate of MCH, mL/min;
ρ is the density of MCH, g/mL;
m is the amount of catalyst used, g;
M is the molar mass of MCH, g/mol;
C is the conversion rate of MCH, %;

S is the selectivity of toluene, %.

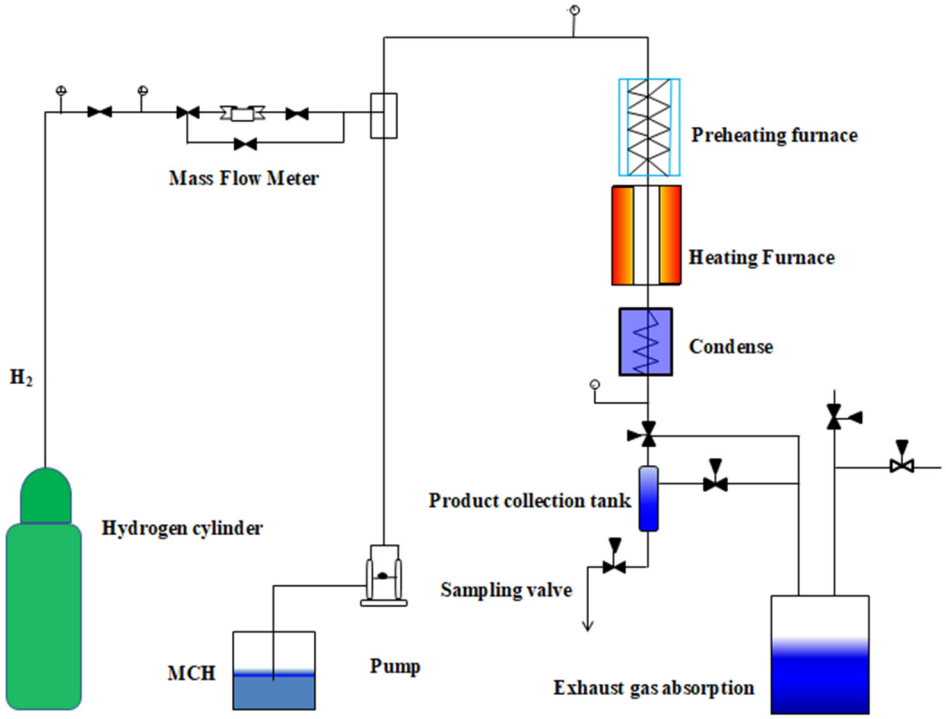


**Figure 9.** Process diagram of catalyst activity evaluation device.

## 4. Conclusions

A series of $Ni_xAl$ catalysts with a high surface area, high dispersion, and small particle size of Ni were prepared by an improved co-precipitation method. The n-butanol-treated precursors can effectively increase the specific surface area and pore capacity of the catalysts, promote the dispersion of nickel species on the carrier, and thus improve the catalytic activity of the catalysts. In addition, the higher specific surface area and NiAlO skeleton structure can also inhibit the agglomeration of nickel species and improve the catalytic stability. The typical catalyst $Ni_{20}Al$ and a comparative catalyst IM-NiAl prepared by the conventional impregnation method were used in the methylcyclohexane dehydrogenation reaction. Under the optimized conditions of T = 450 °C and LHSV = 4 mL $g^{-1}$ $h^{-1}$, the conversion of methylcyclohexane over the $Ni_{20}Al$ catalyst can reach 77.4%, with 85.6% of the selectivity of toluene, 63.94 mmol $g^{-1}$ $h^{-1}$ of the hydrogen release rate, and 29 h of the lifetime of the catalyst, which are all superior to those over the IM-NiAl catalyst prepared by the traditional impregnation method (50.75%, 70.5%, 35.84 mmol $g^{-1}$ $h^{-1}$, and 15 h, respectively).

**Author Contributions:** Conceptualization, Y.Z.; methodology, D.W., Q.L. and H.L.; software, G.L.; data curation, D.W., H.L. and G.L.; writing—original draft preparation, Q.L.; writing—review and editing, D.W. and Q.L.; supervision, Y.Z.; funding acquisition, Y.Z. All authors have read and agreed to the published version of the manuscript.

**Funding:** Financial supports from the National Natural Science Foundation of China (21763016), and industrial support program for colleges and universities in Gansu Province (2020C-06) are acknowledged.

**Data Availability Statement:** Data available on request from the authors.

**Conflicts of Interest:** There are no conflicts to declare.

## References

1. Liu, J.H.; Xu, Z.B.; Jiang, W.; Liu, W.; Guan, X.H. Optimal planning of distributed hydrogen-based multi-energy systems. *Appl. Energy* **2021**, *281*, 116107. [CrossRef]

2. Johnston, B.; Mayo, M.C.; Khare, A. Hydrogen: The Energy Source for the 21st Century. *Technovation* **2005**, *25*, 569–585. [CrossRef]
3. Pradhan, A.; Vishwakarma, M.; Dwivedi, S.K. A review: The impact of hydrogen embrittlement on the fatigue strength of high strength steel. *Mater. Today Proc.* **2020**, *26*, 3015–3019. [CrossRef]
4. Zheng, J.; Liu, X.; Xu, P.; Liu, P.; Zhao, Y.; Yang, J. Development of high pressure gaseous hydrogen storage technologies. *Int. J. Hydrogen Energy* **2012**, *37*, 1048–1057. [CrossRef]
5. Hu, J.; Chandrashekhara, K. Fracture analysis of hydrogen storage composite cylinders with liner crack accounting for autofrettage effect. *Int. J. Hydrogen Energy* **2009**, *34*, 3425–3435. [CrossRef]
6. Ananthachar, V.; Duffy, J.J. Efficiencies of hydrogen storage systems onboard fuel cell vehicles. *Sol. Energy* **2005**, *78*, 687–694. [CrossRef]
7. Zhang, Y.H.; Jia, Z.C.; Yuan, Z.M.; Yang, T.; Yan, Q.I.; Zhao, D.L. Development and application of hydrogen storage. *J. Iron Steel Res. Int.* **2015**, *22*, 757–770. [CrossRef]
8. Biniwale, R.B.; Rayalu, S.; Devotta, S.; Ichikawa, M. Chemical hydrides: A solution to high capacity hydrogen storage and supply. *Int. J. Hydrogen Energy* **2008**, *33*, 360–365. [CrossRef]
9. Bourane, A.; Elanany, M.; Pham, T.V.; Katikaneni, S.P. An over view of organic liquid phase hydrogencarriers. *Int. J. Hydrogen Energy* **2016**, *41*, 23075–23091. [CrossRef]
10. Wang, N.L.; Qiu, J.E.; You, K.Y.; Yuan, X.; Luo, H.A. Microwave assisted synthesis of Sn-modified MgAlO as support for platinum catalyst in cyclohexane dehydrogenation to cyclohexene. *Appl. Catal. A-Gen.* **2016**, *516*, 9–16. [CrossRef]
11. Xia, Z.; Liu, H.; Lu, H.; Zhang, Z. Study on catalytic properties and carbon deposition of Ni-Cu/SBA-15 for cyclohexane dehydrogenation. *Appl. Surf. Sci.* **2017**, *422*, 905–912. [CrossRef]
12. Cromwell, D.K.; Vasudevan, P.T.; Pawelec, B.; Fierro, J. Enhanced methyl cyclhexane dehydrogenation to toluene over Ir/USY catalyst. *Catal. Today* **2016**, *259*, 119–129. [CrossRef]
13. Trimpont, P.A.; Marin, G.B.; Froment, G.F. Kinetics of methylcyclohexane dehydrogenation on sulfided commercial platinum/alumina and platinum –rhenium/alumina catalysts. *Ind. Eng. Chem. Fundam.* **1986**, *25*, 544–553. [CrossRef]
14. Wu, K.; Chen, F.; Wang, F.; Huang, Y.; Yang, Y. Preparation of Pt supported on mesoporous Mg–Al oxide catalysts for efficient dehydrogenation of methylcyclohexane. *Int. J. Hydrogen Energy* **2021**, *46*, 25513–25519. [CrossRef]
15. Sugiura, Y.; Nagatsuka, T.; Kubo, K.; Hirano, Y.; Nakamura, A.; Miyazawa, K.; Iizuka, Y.; Furuta, S.; Iki, H.; Higo, T.; et al. Dehydrogenation of Methylcyclohexane over $Pt/TiO_2$-$Al_2O_3$ Catalysts. *Chem. Lett.* **2017**, *46*, 1601–1604. [CrossRef]
16. Li, X.Y.; Ma, D.; Bao, X.H. Dispersion of Pt Catalysts Supported on Activated Carbon and Their Catalytic Performance in Methylcyclohexane Dehydrogenation. *Chin. J. Catal.* **2008**, *29*, 259–263. [CrossRef]
17. Chen, Y.R.; Tsuru, T.; Kang, D.Y. Simulation and design of catalytic membrane reactor for hydrogen production via methylcyclohexane dehydrogenation. *Int. J. Hydrogen Energy* **2017**, *42*, 26296–26307. [CrossRef]
18. Yakovlev, V.A.; Gulyaeva, Y.K.; Alekseeva, M.V.; Ermakov, D.Y.; Bulavchenko, O.A.; Zaikina, O.O. High-Loaded Nickel Based Sol–Gel Catalysts for Methylcyclohexane Dehydrogenation. *Catalysts* **2020**, *10*, 1198.
19. Ham, H.; Simanullang, W.F.; Kanda, Y.; Wen, Y.; Hashimoto, A.; Abe, H.; Shimizu, K.I.; Furukawa, S. Silica-Decoration Boosts Ni Catalysis for (De)hydrogenation: Step-Abundant Nanostructures Stabilized by Silica. *ChemCatChem* **2021**, *13*, 1306–1310. [CrossRef]
20. Yolcular, S. Organic chemical hydride dehydrogenation over nickel catalysts supported with $SiO_2$ for hydrogen recovery. Energy Sources Part A: Recovery. *Util. Environ. Eff.* **2016**, *14*, 2031–2034.
21. Al-Shaikhali, A.H.; Jedidi, A.; Anjum, D.H.; Cavallo, L.; Takanabe, K. Kinetics on NiZn Bimetallic Catalysts for Hydrogen Evolution via Selective Dehydrogenation of Methylcyclohexane to Toluene. *ACS Catal.* **2017**, *7*, 1592–1600. [CrossRef]
22. Meng, J.C.; Zhou, F.; Ma, H.X.; Yuan, X.Z.; Wang, Y.Z.; Zhang, J. A Review of Catalysts for Methylcyclohexane Dehydrogenation. *Top. Catal.* **2021**, *64*, 509–520. [CrossRef]
23. Zhu, C.; Chen, S.; Pan, D.; Cui, X.; Qiao, Y.; Li, R. Ordered mesoporous alumina-supported vanadium oxides as an efficient catalyst for ethylbenzene dehydrogenation to styrene with $CO_2$. *Catal. Commun.* **2018**, *115*, 12–16. [CrossRef]
24. Zhao, Y.; Wang, J.E.; Chen, H.; Zhang, X.Y.; Fu, Y.C.; Shen, J.Y. Synthesis of high-surface-area Co-O-Si compl:ex oxide for skeletal isomerization of 1-hexene and hydrodesulfurization of thiophene. *Chin. J. Catal.* **2014**, *35*, 1402–1409. [CrossRef]
25. Zhao, Y.; Wang, J.E.; Song, G.X.; Shen, J.Y.; Tian, X.C. Preparation of $NiAlO_x$ and $NiSiO_x$ Complex Oxides with High Surface Areas for the Isomerization Reactions of 1-Hexene. *Catal. Lett.* **2016**, *146*, 1934–1942. [CrossRef]
26. Song, K.H.; Jeong, S.K.; Jeong, B.H.; Lee, K.Y.; Kim, H.J. Effect of the Ni/Al ratio on the performance of $NiAl_2O_4$ spinel-based catalysts for supercritical methylcyclohexane catalytic cracking. *Catalysts* **2021**, *11*, 323. [CrossRef]
27. Li, L.; Hui, K.S.; Hui, K.N.; Cho, Y.R. Ultrathin petal-like NiAl layered doubleoxide/sulfide composites as an advanced electrode for high-performance asymmetric supercapacitors. *J. Mater. Chem. A* **2017**, *5*, 19687–19696. [CrossRef]
28. Vandergrift, C.; Elberse, P.A.; Mulder, A.; Geus, J.W. Preparation of Silica- supported Copper Catalysts by Means of Deposition-precipitation. *Appl. Catal.* **1990**, *59*, 275–289. [CrossRef]
29. Gervasini, A.; Manzoli, M.; Martra, G.; Ponti, A.; Ravasio, N.; Sordelli, L.; Zaccheria, F. Dependence of Copper Species on the Nature of the Support for Dispersed CuO Catalysts. *J. Phys. Chem. B* **2006**, *110*, 51–61. [CrossRef]
30. Chen, Z.; Yang, Y.Q.; Bao, J.G.; Wang, W.Y.; Jiang, X.M. Catalytic performance of $Ni/\gamma$-$Al_2O_3$ for hydrogen carrier methylcyclohexane dehydrogenation. *Chem. Ind. Eng. Prog.* **2010**, *29*, 484–489.

31. Shukla, A.A.; Gosavi, P.V.; Pande, J.V.; Kumar, V.P.; Chary, K.; Biniwale, R.B. Efficient hydrogen supply through catalytic dehydrogenation of methylcyclohexane over Pt/metal oxide catalysts. *Int. J. Hydrogen Energy* **2010**, *35*, 4020–4026. [CrossRef]
32. Jing, Y.; Wang, W.; Lei, M.; Wu, K.; Chen, G.; Huang, Y. Dehydrogenation of methylcyclohexane over Pt Sn supported on Mg Al mixed metal oxides derived from layered double hydroxides. *Int. J. Hydrogen Energy* **2018**, *43*, 9343–9352.
33. Li, G.H.; Xiong, G.; Zhao, X.; Wang, W.Y.; Li, W.S.; Yang, Y.Q. Ni-Cu/$\gamma$-$Al_2O_3$-$ZrO_2$ preparation of catalyst and its dehydrogenation performance. *Petrochem. Technol.* **2016**, *45*, 798–804.